Cospectral budget of turbulence explains the bulk properties of smooth pipe flow

Gabriel G. Katul[1,2] and Costantino Manes[3]
[1]*Nicholas School of the Environment, Duke University, Durham, North Carolina 27708-0328, USA*
[2]*Department of Civil and Environmental Engineering, Duke University, Durham, North Carolina 27708, USA*
[3]*Faculty of Engineering and the Environment, University of Southampton, Southampton SO171BJ, United Kingdom*
(Received 10 June 2014; published 10 December 2014)

Connections between the wall-normal turbulent velocity spectrum $E_{ww}(k)$ at wave number k and the mean velocity profile (MVP) are explored in pressure-driven flows confined within smooth walls at moderate to high bulk Reynolds numbers (Re). These connections are derived via a cospectral budget for the longitudinal (u') and wall-normal (w') velocity fluctuations, which include a production term due to mean shear interacting with $E_{ww}(k)$, viscous effects, and a decorrelation between u' and w' by pressure-strain effects [$=\pi(k)$]. The $\pi(k)$ is modeled using a conventional Rotta-like return-to-isotropy closure but adjusted to include the effects of isotropization of the production term. The resulting cospectral budget yields a generalization of a previously proposed "spectral link" between the MVP and the spectrum of turbulence. The proposed cospectral budget is also shown to reproduce the measured MVP across the pipe with changing Re including the MVP shapes in the buffer and wake regions. Because of the links between $E_{ww}(k)$ and the MVP, the effects of intermittency corrections to inertial subrange scales and the so-called spectral bottleneck reported as k approaches viscous dissipation eddy sizes (η) on the MVP shapes are investigated and shown to be of minor importance. Inclusion of a local Reynolds number correction to a parameter associated with the spectral exponential cutoff as $k\eta \to 1$ appears to be more significant to the MVP shape in the buffer region. While the bulk shape of the MVP is reasonably reproduced in all regions of the pipe, the solution to the cospectral budget systematically underestimates the negative curvature of the MVP within the buffer layer.

DOI: 10.1103/PhysRevE.90.063008 PACS number(s): 47.27.N−

I. INTRODUCTION

Pressure-driven flows at high bulk Reynolds numbers (Re) within smooth walls continue to receive significant experimental [1–8] and theoretical [9–12] attention. A recent phenomenological theory, labeled the "spectral link" [11], unfolded a number of features about the shape of the mean velocity profile (MVP) in smooth pipes from the shape of the turbulent kinetic energy spectrum $E_{\mathrm{TKE}}(k)$, where k is a wave number or inverse eddy size. In particular, the spectral link showed qualitatively that curvatures in the MVP within the buffer layer are connected to the exponential correction of $E_{\mathrm{TKE}}(k)$ at large k due to viscous effects, the logarithmic MVP within the intermediate region is linked with the inertial subrange scaling of $E_{\mathrm{TKE}}(k)$ commonly described by Kolmogorov's theory [13,14] in the absence of intermittency corrections [9,15], and the wake effects where the MVP "overshoots" the logarithmic shape appear to be attributed to the so-called von Kármán spectrum describing $E_{\mathrm{TKE}}(k)$ at k commensurate with the inverse of the pipe radius $1/R$. The spectral link is based on the argument that the turbulent stress τ_t at a distance y from a wall is given by the product of a mean velocity difference reflecting a momentum deficit across an eddy of radius s and its turnover velocity given as [11]

$$\tau_t \sim v_s \left[U(y+s) - U(y-s)\right], \tag{1}$$

where $U(y)$ is the mean velocity at distance y from the boundary, v_s is a turnover velocity for an eddy of radius s centered at some position x and height y whose order of magnitude can be predicted from $v_s = \int_{1/s}^{\infty} E_{\mathrm{TKE}}(k)dk$, and $U(y+s) - U(y-s) \approx (dU/dy)(2s)$ is the mean velocity difference associated with this momentum transporting eddy size. The proposed spectral link further assumes that only eddies attached to the wall efficiently transport momentum [11], thereby setting $2s = y$. These arguments have established a phenomenological framework that links the turbulent momentum flux to the MVP via $E_{\mathrm{TKE}}(k)$, thereby offering new vistas to explaining the shape of the MVP from the shape of $E_{\mathrm{TKE}}(k)$. However, the spectral link between v_s and $E_{\mathrm{TKE}}(k)$ used by Gioia and co-workers is somewhat ad-hoc. In particular, since the velocity gradient is dictated by vertical momentum transport (i.e., v_s is a vertical velocity scale), it is not clear why v_s should be related to the TKE spectrum [i.e., $E_{\mathrm{TKE}}(k)$] and not the vertical velocity spectrum [i.e., $E_{ww}(k)$], which are notoriously different, especially in the energy-containing range (i.e., for small k). Furthermore, linearizing $U(y+s) - U(y-s) \approx (dU/dy)(2s)$ is only reasonable for small s, and it is not evident why only eddies whose size $2s = y$ contribute to $U(y+s) - U(y-s)$. The assumption $v_s = \int_{1/s}^{\infty} E_{\mathrm{TKE}}(k)dk$ is also questionable. In fact, within a phenomenological context, the velocity scale v_s could or should be interpreted as the velocity variation across a distance $2s$, which can be predicted from the second-order velocity structure function computed at a distance $2s$, i.e.,

$$v_s^2 = \overline{|\Delta w'(2s)|^2} = \overline{|w'(x+s) - w'(x-s)|^2}, \tag{2}$$

where w' is the vertical velocity fluctuation, and the overbar denotes time-averaging. As shown by [16], the structure function and the spectrum of a velocity component are related by the following relation:

$$\overline{|\Delta w'(s)|^2} \approx \frac{4}{3}\int_{\pi/s}^{\infty} E_{ww}(k)dk + \frac{4}{3}\frac{s^2}{\pi^2}\int_0^{\pi/s} k^2 E_{ww}(k)dk, \tag{3}$$

where the first term includes all the energy in eddies of size s or smaller, while the second term includes all the enstrophy-like terms in eddies of size s or larger [enstrophy $\omega^2 = \int_0^\infty p^2 E_{\mathrm{TKE}}(p)dp$]. The approximation employed by Gioia and co-workers [11] to link $\overline{|\Delta w'(s)|^2}$ to a turbulent energy spectrum replaces $E_{ww}(k)$ with $E_{\mathrm{TKE}}(k)$ and ignores contributions from the enstrophy term.

An alternative formulation that maintains the analytical tractability of the spectral link between the MVP and an energy spectrum but relaxes some of these restrictive assumptions frames the scope of this work. This alternative formulation recovers many theoretical features of the spectral link [11] but uses a cospectral budget for the longitudinal and wall-normal velocity fluctuations. It is shown that the previously proposed spectral link of Gioia and co-workers [11] naturally arises from the production term in this cospectral budget. This production term is determined by dU/dy instead of $[U(y+s) - U(y-s)]$ and $E_{ww}(k)$ instead of $E_{\mathrm{TKE}}(k)$, and eddies of all sizes are accounted for in momentum transfer to the wall. The proposed cospectral budget is shown (i) to be consistent with the onset of a $-7/3$ power-law scaling in the cospectrum between longitudinal and wall-normal velocity fluctuations for eddies within the inertial subrange (not discussed for the previously proposed spectral link by Goia and co-workers [11]), and (ii) to reproduce the MVP across all regions in the pipe with changing Re as reported experimentally [5,6].

II. THEORY

A. Definitions and general considerations

Consider the pressure-driven flow in a smooth pipe with radius R having a cross-sectional area $A_p = \pi R^2$ as shown in Fig. 1. Let $y = R - r$ be the normal distance to the boundary, r the distance from the pipe center, $U^+ = U(y)/u_\tau$ the dimensionless mean velocity profile, $u_\tau = (\tau_o/\rho)^{1/2}$ the friction (or shear) velocity, τ_o the total wall stress, ρ the fluid density, $y^+ = yu_\tau/\nu$ the dimensionless distance from the boundary, ν the fluid kinematic viscosity, $R^+ = Ru_\tau/\nu$ the von Kármán number, U_b the bulk (or area-averaged)

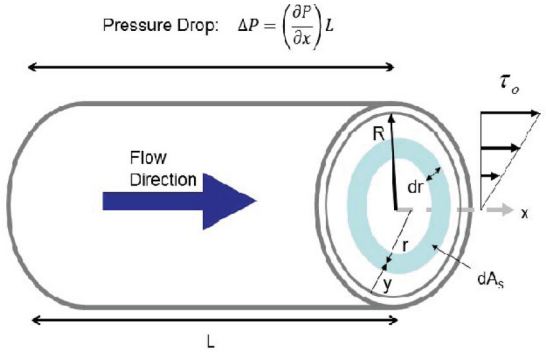

FIG. 1. (Color online) Schematic of the smooth-walled pipe flow configuration showing the pipe length L, pipe radius R, distance from the wall $y = R - r$, distance from the pipe center r, and the resulting total stress distribution when the pressure gradient $(\partial P/\partial x)$ is assumed constant.

velocity defined as $U_b = (1/A_p)\int_0^R U(r)dA_s$, where $dA_s = 2\pi r dr$, and $\mathrm{Re} = U_b D/\nu$ the bulk Reynolds number based on pipe diameter $D = 2R$. For a stationary and longitudinally homogeneous pipe flow driven by a constant mean pressure gradient, the mean longitudinal momentum balance reduces to

$$\frac{1}{\rho}\frac{\partial P}{\partial x} = \frac{1}{r}\frac{\partial (r\tau)}{\partial r}, \tag{4}$$

where P is the mean pressure, x is the longitudinal distance along the pipe length, and τ is the total shear stress.

Integrating with respect to r for a constant pressure gradient results in

$$\tau(r) = \frac{1}{\rho}\left(\frac{\partial P}{\partial x}\right)\frac{r}{2} + C_1, \tag{5}$$

where C_1 is determined so that at $r = R$ (center of the pipe), $\tau(R) = 0$ due to symmetry, thereby resulting in

$$\tau(r) = \frac{1}{\rho}\left(\frac{\partial P}{\partial x}\right)\frac{r}{2} = \frac{R}{2}\left(\frac{\partial P}{\partial x}\right)\left(1 - \frac{y}{R}\right). \tag{6}$$

Defining

$$\tau_o = \frac{R}{2}\left(\frac{\partial P}{\partial x}\right), \tag{7}$$

and decomposing the τ into a turbulent τ_t and a viscous τ_m contribution, leads to

$$\tau(y) = \tau_t + \tau_m = \tau_o\left(1 - \frac{y}{R}\right), \tag{8}$$

with $\tau_m = \rho\nu\Gamma(y)$ and $\Gamma(y) = dU/dy$. The τ_t is defined as

$$\tau_t = -\rho\overline{u'w'} = -\rho\int_0^\infty F_{wu}(k)\,dk, \tag{9}$$

where u' is the turbulent longitudinal velocity component, $F_{wu}(k)$ is the one-dimensional cospectrum between u' and w', and k is, as before, a wave number quantifying an eddy of size $1/k$. Hence, the mean momentum balance reduces to

$$\nu\Gamma + \int_0^\infty F_{wu}(k)\,dk = \frac{\tau_o}{\rho}\left(1 - \frac{y}{R}\right). \tag{10}$$

Close to the wall boundary (i.e., $y^+ \ll 5$), $\tau_t \ll \tau_m$ and $\Gamma = (\tau_o/\rho\nu)(1 - y/R)$, which upon integration results in the well-known parabolic velocity profile given as $U(y) = (\tau_o/\rho\nu)\,y\,(1 - y/D)$ in the viscous region of the pipe. However, for $y/D \ll 1$, the mean velocity profile reduces to its linear form given by $U(y) \approx (\tau_o/\rho\nu)\,y$. This MVP is used to connect the wall stress to $U(y)$ up to $y^+ = 1$.

B. The cospectral budget

Beyond this thin region adjacent to the smooth wall surface $(0 \leqslant y^+ \leqslant 1)$, $\rho\overline{u'w'}$ is not negligible relative to τ_m, and its effects must be explicitly accounted for. Processes governing the wall-normal variations in $\overline{u'w'}$ can be identified through the turbulent stress budget. For a stationary pipe flow, the turbulent stress budget is expressed as follows [17]:

$$\frac{\partial\overline{u'w'}}{\partial t} = \mathrm{PR} + \mathrm{PS} + \mathrm{DS} + \mathrm{TD} + \mathrm{PD} + \mathrm{VD}, \tag{11}$$

where t is time, PR is the production term, PS is the pressure strain, DS is dissipation, TD is turbulent diffusion, PD is pressure diffusion, and VD is viscous diffusion. In turbulent shear flows, the PR and PS terms are known to provide the leading contributions to the stress budget, while the other terms become non-negligible only in the near wall region [17,18]. In view of these observations, and to retain maximum simplicity, an abridged stress budget with an interplay between production and pressure strain terms is considered. However, the dissipation term is also retained, which, as will be shown later, provides the means of establishing the cospectral link with the mean velocity profile in the buffer region. Therefore, this approximated stress budget now reads

$$\frac{\partial \overline{u'w'}}{\partial t} = 0 = -\sigma_w^2 \Gamma + \overline{\frac{p'}{\rho}\left(\frac{\partial u'}{\partial y} + \frac{\partial w'}{\partial x}\right)} + \mathrm{DS}, \qquad (12)$$

where p' is the turbulent pressure perturbation. The first two terms on the right-hand side represent production (PR) and pressure strain (PS), respectively (the full mathematical formulation for the dissipation term is omitted for brevity but can be found elsewhere [17]).

A cospectral budget that reflects a balance among these terms is given as [15,19,20]

$$\frac{\partial F_{wu}(k)}{\partial t} + 2\nu k^2 F_{wu}(k) = G(k), \qquad (13)$$

where $G(k) = P_{wu}(k) + \pi(k)$, $P_{wu} = \Gamma E_{ww}(k)$ is the production term, where $\int_0^\infty P_{wu}(k)dk = -\sigma_w^2\Gamma$, $E_{ww}(k)$ is the energy spectrum [$\sigma_w^2 = \int_0^\infty E_{ww}(k)dk$], $\mathrm{DS} = -\frac{1}{2}\nu\int_0^\infty k^2 F_{wu}(k)dk$ is viscous dissipation of $\overline{u'w'}$, and $\pi(k)$ is the velocity-pressure interaction term satisfying the normalizing property

$$\int_0^\infty \pi(k)dk = \overline{\frac{p'}{\rho}\left(\frac{\partial u'}{\partial y} + \frac{\partial w'}{\partial x}\right)}, \qquad (14)$$

which acts to decorrelate u' from w' as discussed elsewhere [18]. In conventional second-order closure modeling, this term is closed via the so-called LRR-IP formulation given as

$$\int_0^\infty \pi(k)dk = -C_R\frac{1}{T}(\overline{u'w'}) + C_I\sigma_w^2\Gamma(y), \qquad (15)$$

where LRR stands for Launder-Reece-Rodi (LRR) and IP stands for the isotropization of the production [21] that was proposed as a correction to the Rotta [22] model based on rapid distortion theory [18], $T = K/\epsilon$ is a relaxation time scale, K is the turbulent kinetic energy as before, ϵ is the mean dissipation rate of K, $C_R \approx 1.8$ is the Rotta constant, and C_I is a constant associated with the isotropization of the production term correcting the original Rotta model [18,23]. Its value $C_I = 3/5$ was previously predicted from rapid distortion theory for isotropic turbulence [18,21] as well as early numerical simulations [24]. This closure formulation for the pressure-velocity interaction term is employed here because of its ability to reproduce $\int_0^\infty \pi(k)dk$ for homogeneous shear flows [18]. When inhomogeneous flows in the axial direction are encountered, issues with this closure scheme have been studied for rapid axisymmetric expansion or contraction. In these types of axisymmetric flows, cigar-shaped versus pancake-shaped componentwise energy ellipsoids relax to isotropy at different rates [23], and these rates were shown not to be much faster than T. Other simulation studies [24] suggest that the Rotta closure is valid as long as the time scale of the mean flow is much larger than $0.2l_f/[(2K)^{1/2}]$, where l_f is the integral time scale of the flow, and the quantity $0.2l_f/[(2K)^{1/2}]$ represents a characteristic time scale of the triple moments [24]. Not withstanding these issues, and noting that the LRR-IP model proved accurate for many wall-bounded flows where the return to isotropy was sufficiently fast compared to T [18,24,25], then

$$\pi(k) = -C_R\frac{F_{wu}(k)}{\tau(k)} + C_I P_{wu}(k), \qquad (16)$$

where $\tau(k) = \epsilon^{-1/3}k^{-2/3}$ is a wave-number-dependent relaxation time scale that varies with k and ϵ consistent with Kolmogorov's theory (or K41) in the inertial subrange [13,14]. This wave-number-dependent relaxation time scale, attributed to Onsager [26] by Corrsin [27], has been extensively used in many turbulence theories [19,24,28–34]. Employing this conventional approximation for $\pi(k)$ and $\tau(k)$, the cospectral budget reduces to

$$2\nu k^2 F_{wu}(k) = (1 - C_I)\,\Gamma(y)E_{ww}(k) - C_R\frac{F_{wu}(k)}{\tau(k)}. \qquad (17)$$

The relative importance of the Rotta component and the viscous term $2\nu k^2 F_{wu}(k)$ in the cospectral budget can be estimated from

$$\frac{2\nu k^2 F_{wu}(k)}{C_R F_{wu}(k)/\tau(k)} = \frac{2}{C_R}\left(\frac{\nu^3 k^4}{\epsilon}\right)^{1/3} \approx (k\eta)^{4/3}, \qquad (18)$$

where $\eta = (\nu^3/\epsilon)^{1/4}$ is the Kolmogorov microscale [35]. For $k\eta \ll 1$, decorrelation between u' and w' due to molecular effects can be ignored relative to the Rotta term. However, as $k\eta \to 1$, these two decorrelation terms become comparable in magnitude, as may occur in the lower portion of the buffer region.

C. The intermediate region

This region has been the subject of a recent investigation using the cospectral budget [15], and only the salient features are reviewed. Consider the region where $y^+ \gg 10$ but $y/R \ll 1$ so that $\tau_t \approx \tau_o$. Assuming stationary conditions and upon further ignoring the pressure and the turbulent and viscous diffusion terms, the cospectral budget reduces to a balance between production and pressure strain terms leading to

$$F_{wu}(k) = \frac{1}{A}\Gamma\epsilon^{-1/3}E_{ww}(k)\,k^{-2/3}, \qquad (19)$$

where $A = C_R/(1 - C_I) = 1.8/[1 - (3/5)] \approx 4.5$. As far as the intermediate region is concerned, neglecting diffusion terms in the stress budget equation is an approximation that is well supported by a large body of literature (see, e.g., [36,37]), and hence ignoring their effects in the cospectral budget may be viewed as plausible. When $E_{ww}(k)$ is given by its K41 phenomenological form [13], $E_{\mathrm{Kol}}(k) = C'_K\epsilon^{2/3}k^{-5/3}$, generally valid for $\eta \ll k^{-1} \ll y$, then

$$F_{wu}(k) = \frac{C'_K}{A}\Gamma\epsilon^{\frac{1}{3}}k^{-\frac{7}{3}}. \qquad (20)$$

The $F_{wu}(k)$ expression agrees with $F_{wu}(k) = C_{uw}\Gamma\epsilon^{1/3}k^{-7/3}$ first derived by Lumley [38] from dimensional considerations. This cospectral scaling rule is now supported by measurements in the high Reynolds number pipe, the boundary layer, and atmospheric flows [18,34,39]. The value of $C'_K = (24/55)C_K$, where $C_K \approx 1.5$ is the Kolmogorov constant associated with three-dimensional wave numbers and leads to $C_{uw} = C'_K/A \approx 0.65/4.5 = 0.15$. This C_{uw} estimate is sufficiently close to the accepted $C_{uw} = 0.15$–0.16 [15,18,40] directly estimated from measured $F_{wu}(k)$ (in one dimension) and $\Gamma(y)$.

To recover a "spectral link" between $E_{ww}(k)$ and $U(y)$ analogous (but not identical) to the one previously proposed by Gioia and co-workers [11], the mean momentum balance $\int_0^\infty F_{uw}(k)\,dk \approx \tau_o/\rho$ is considered again within the intermediate region. The $F_{wu}(k)$ requires a description of $E_{ww}(k)$ across all k. An idealized $E_{ww}(k)$ that is constant for $k \leqslant k_a$ and abruptly switches to inertial subrange scaling for $k \geqslant k_a$ is assumed and is shown in Fig. 2. Exponential corrections (or a variant of them known as the Pao correction [18,39]) such as $k\eta \to 1$ and low-wave-number modulations such as $kR \to 1$ are momentarily ignored in the assumed $E_{ww}(k)$ shape. The two regions delineating the idealized shape of $E_{ww}(k)$ in Fig. 2 are supported by a large corpus of data collected across many field and laboratory experiments [18]. This idealized spectral shape for $E_{ww}(k)$ with its "breakpoint" at $k_a y = 1$ is also consistent with Townsend's attached eddy hypothesis [3,41,42]. With this description for $E_{ww}(k)$,

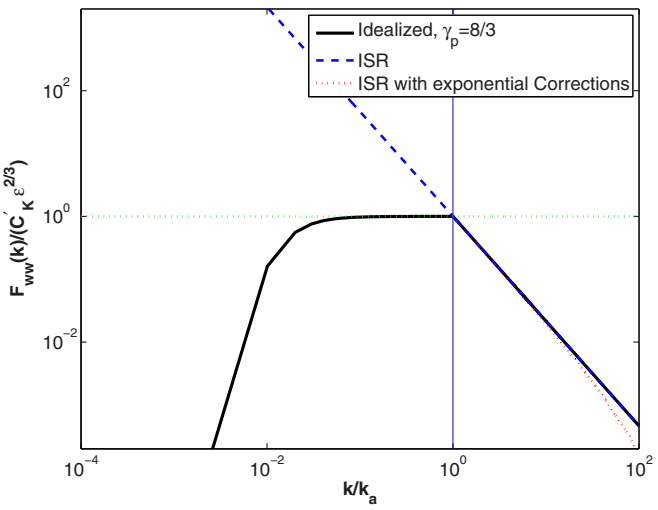

FIG. 2. (Color online) The idealized vertical velocity spectrum $E_{ww}(k)$ assumed in the calculations of $F_{wu}(k)$. Much of the energy in the vertical velocity variance (σ_w^2) is contained in two regimes, a near constant regime for $k < k_a$ and inertial subrange scaling for $k > k_a$ given by K41 scaling. The exponential corrections $\exp(-\beta_d\eta k)$ shown here for $\beta_d = 5.2$ become significant near the viscous subrange as $k\eta \to 1$, while very-low-wave-number modulations reduce $E_{ww}(k_a)$ from its constant value to $\phi_p(kR)$ as $kR \to 1$. Here, $\phi_p(kR) = [1 + (Rk)^{-2}]^{-\gamma_p}$ for the case $\gamma_p = 8/3$ is shown. The idealized two-regime spectrum (constant and inertial) used in the analysis of the intermediate region is for $\beta_d = 0$ and $\gamma_p = 0$.

$\int_0^\infty F_{wu}(k)dk$ is given as

$$\tau_o/\rho = u_\tau^2 = C_{uw}\Gamma\epsilon^{1/3}\left(\int_0^{k_a} k_a^{-7/3}dk + \int_{k_a}^{\infty} k^{-7/3}dk\right), \tag{21}$$

resulting in

$$u_\tau^2 = \frac{7C_{uw}}{4}\Gamma\epsilon^{1/3}{k_a}^{-4/3}. \tag{22}$$

In the intermediate region, $\epsilon = \Gamma u_\tau^2$ and $k_a = y^{-1}$ so that the above expression for u_τ^2 can be rearranged to yield

$$\Gamma = \left(\frac{4}{7C_{uw}}\right)^{3/4}\frac{u_\tau}{y}, \tag{23}$$

which upon integration with respect to y yields the log-law,

$$\frac{U(y)}{u_\tau} = \left(\frac{4}{7C_{uw}}\right)^{3/4}\ln(y) + B_o, \tag{24}$$

where B_o is an integration constant that varies with surface properties. The constant $[(4/7)C_{uw}^{-1}]^{3/4} = 2.7$ is close to the expected values of $1/\kappa$ observed in the literature (i.e., $2.3 \leqslant 1/\kappa \leqslant 2.6$; see [18]), where κ is the von Kármán constant. This provides confidence in the LRR-IP formulation and its associated constants adopted here.

D. The entire pipe region: A spectral integration

In general, τ_t and τ_m are both significant for $\eta < r \leqslant R$ depending on the pipe region and Re. From the approximated cospectral budget with an imposed $E_{ww}(k)$ given in Fig. 2, the cospectrum is expressed as

$$F_{wu}(K) = \frac{(1 - C_I)\Gamma E_{ww}(k)}{\left[2\nu k^2 + \frac{C_R}{\tau(k)}\right]}. \tag{25}$$

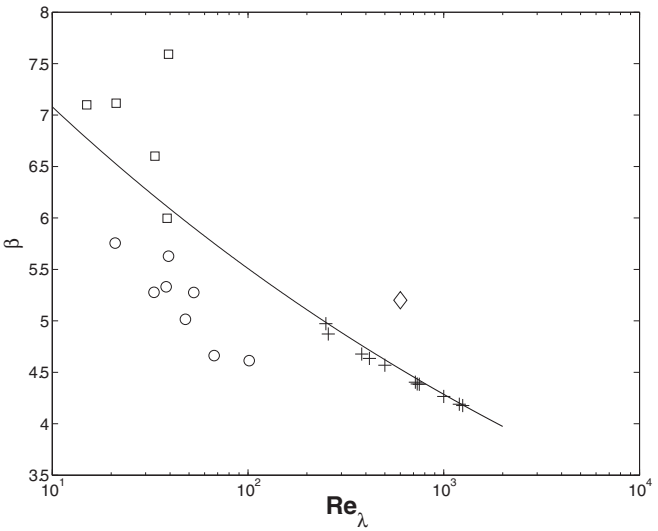

FIG. 3. Variations of β_d with Re_λ reported across several simulation studies. Circles and squares are taken from [43], pluses are taken from high-resolution direct numerical simulations in [44], and diamond is from a wind-tunnel experiment [39]. The line $\beta_d \approx 9.1\,\mathrm{Re}_\lambda^{-0.1}$ is also shown and used in the cospectral calculations of the MVP.

The exponential cutoff as $k\eta \to 1$ and low-wave-number modulations $\phi_p(k)$ as $kR \to 1$ are now included in $E_{ww}(k)$ as shown in Fig. 2. Hence,

$$E_{ww}(K) = \phi_p(kR)\min\begin{cases} E_{\rm kol}(k)[\exp(-\beta_d \eta k)], \\ E_{\rm kol}(k_a)[\exp(-\beta_d \eta k_a)], \end{cases} \quad (26)$$

where $k_a = (1/y)$ as before and β_d is the coefficient of the exponential correction to $E_{ww}(k)$ in the viscous range [39]. When combining several studies together, β_d appears to vary with the Taylor microscale Reynolds number Re_λ given by

$$\mathrm{Re}_\lambda = \frac{\lambda' \sigma_w}{\nu}, \quad \lambda' = \left(\frac{15\nu}{\epsilon}\sigma_w^2\right)^{1/2}, \quad (27)$$

where λ' is the Taylor microscale and σ_w can be determined by integrating $E_{ww}(k)$ across all k as noted earlier. Upon fitting a power dependence of β_d on Re_λ using simulation runs reported in previous studies [39,43,44], a $\beta_d \approx 9.1\,\mathrm{Re}_\lambda^{-0.1}$ captures this dependence as shown in Fig. 3.

Because there is little experimental information about the behavior of $E_{ww}(k)$ for $kR < 1$, and to ensure that as $k \to 0$, $E_{ww}(0) = 0$, we assumed $\phi_p(kR) = [1 + (Rk)^{-2}]^{-\gamma_p}$, where $\gamma_p \geqslant 0$. This adjustment leads to a decline in $E_{ww}(k)$ with increasing eddy sizes when eddies become much larger than R. When $\gamma_p = 0$, $\phi_p(kR) = 1$ and no low-wave-number modulations to the constant $E_{ww}(k_a)$ are allowed. On the other hand, if a von Kármán–like spectrum approximating $E_{\rm TKE}(k)$ at low k is employed as in the original spectral link [11], $\gamma_p = 17/6$. As discussed elsewhere [11], it is the $\phi_p(kR)$ that dictates the shape of the wake region in $U(y)$. A $\gamma_p = 8/3$ is selected to reflect some modulations at low k. This choice is an intermediate between what was used by Gioia and co-workers [11], proposed elsewhere [44] based on high-resolution DNS, and what was experimentally reported from the Superpipe experiments [45] about a near-constant $E_{ww}(k)$ in the vicinity of $kR \approx 1 - 10$. For this prescribed $E_{ww}(k)$ shape, the resulting mean momentum balance is given by

$$\int_0^\infty \frac{(1 - C_I)\Gamma E_{ww}(k)}{\left[2\nu k^2 + \frac{C_R}{\tau(k)}\right]} dk = \left[\tau_o\left(1 - \frac{y}{R}\right) - \nu\Gamma\right], \quad (28)$$

necessitating an iterative procedure for computing $\Gamma(y)$ at each y given that ϵ and η in the exponential corrections to $E_{ww}(k)$ both vary with Γ.

Upon vertically integrating the computed $\Gamma(y)$ with respect to y, $U(y)$ can be determined and shown in Figs. 4 and 6 for various Re. Agreement between measured and modeled U^+ is encouraging. Despite its simplicity, the proposed model is able to reproduce all the complex features of $U(y)$. These features include a buffer layer, an intermediate-log layer, and a wake region characterized by the typical overshoot in velocities, commonly referred to as Cole's wake effect. There are two regions where the model deviates from the measured $U(y)$. The first is in the buffer region (see Fig. 5), where the negative curvature in the MVP appears slightly underestimated and the second region is near the centerline. Possible explanations

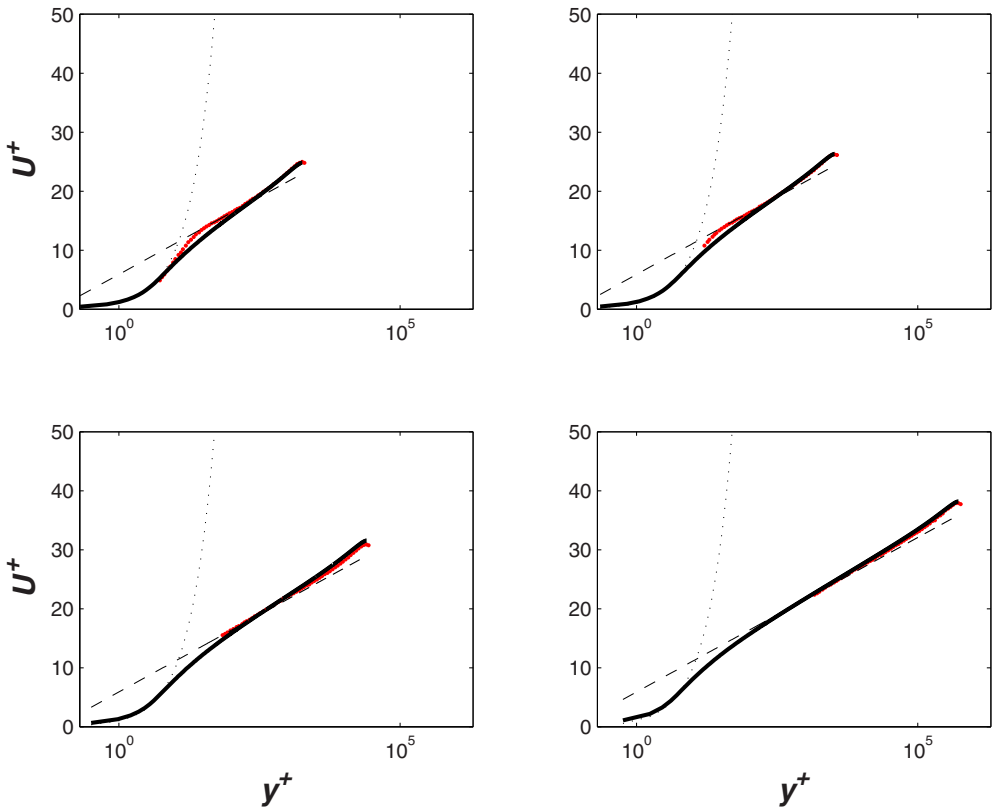

FIG. 4. (Color online) Comparison between measured (symbols) and modeled (solid line) profiles of U^+ as a function of wall distance y^+ (left) using Eq. (28) across selected $\mathrm{Re} = 7.43 \times 10^4$, 1.45×10^5, 1.80×10^6, and 3.57×10^7. Measurements are from the Superpipe experiment [5,6]. The parabolic (dots) and logarithmic (dashed) profiles with $\kappa = 0.44$ as reported by [5,6] are shown for reference.

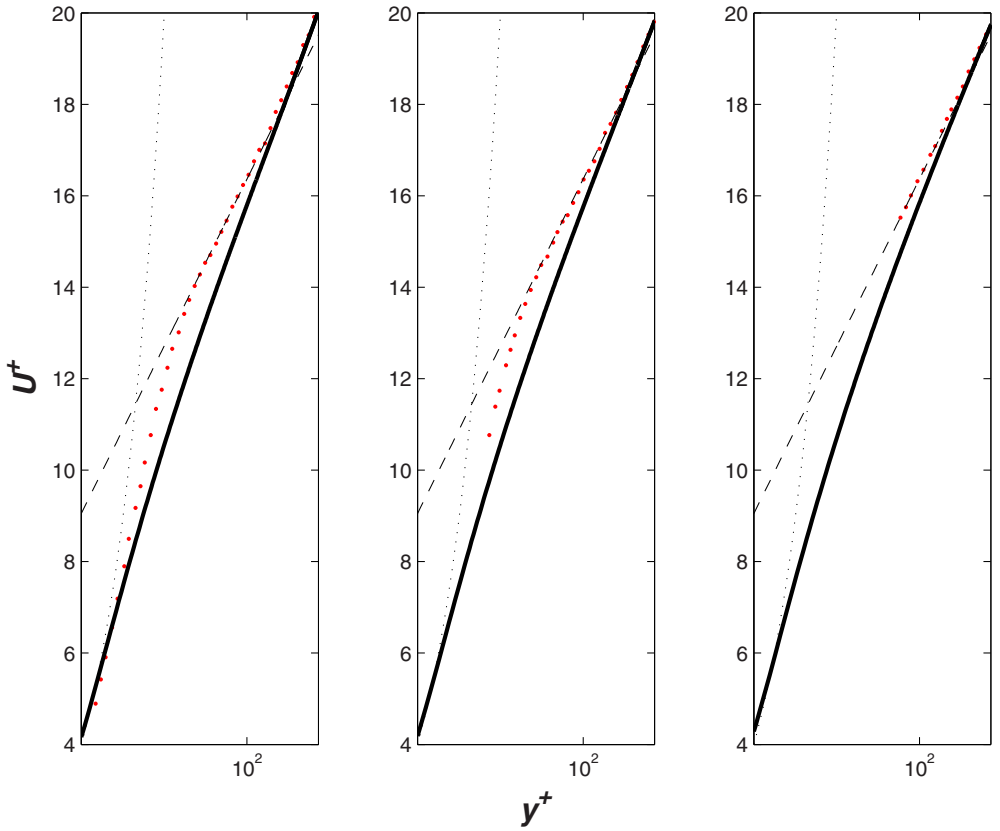

FIG. 5. (Color online) Same as Fig. 4 but zooming in on the buffer region. Since no measurements are reported in the buffer region for $\mathrm{Re} = 3.57 \times 10^7$, it is not included in the zoom-in.

can be offered as a mix of different effects and are now discussed. First of all, within the buffer region, the diffusion terms in the Reynolds stress (and hence cospectral) budget, although small, are not entirely negligible, and this can have an effect on determining the shape of the mean velocity profile. As is evident from Eq. (26), intermittency corrections to K41 [14,46–48] and bottleneck effects [44,49–52] have been ignored in the formulation of $E_{ww}(k)$. These adjustments have been added to the idealized $E_{ww}(k)$ using simplified expressions [44], and their joint contribution was shown to be of secondary importance to the negative curvature in $U(y)$ (not shown). Another assumption employed here is the constant $C_R = 1.8$, but its Reynolds number dependence may be significant [53,54]. Analysis reported elsewhere [54] suggests increasing C_R with increasing turbulent Reynolds number (connected to but not identical to Re_λ) until a saturation value of 2.6 is reached (occurring at infinite Reynolds number). A sensitivity analysis conducted here suggest that the negative curvature in $U(y)$ within the buffer region can be indeed amplified but for a C_R decreasing with increasing Re_λ. The assumption $\epsilon = \Gamma\tau_t$, which is known not to hold in the buffer or the wake regions, can be more restrictive. This assumption is difficult to relax using an equilibrated TKE budget as assumed here and as done earlier by Gioia and co-workers in their derivation of the spectral link [11]. Another region where the model appears to not reproduce well the measurements is in the immediate vicinity of the pipe centerline. This is not surprising, because $\Gamma = 0$ (by symmetry) at the pipe centerline modeled $\epsilon = 0$ when using an equilibrium TKE budget resulting in an unrealistic $\sigma_w = 0$ as shown in Fig. 6. Near the centerline and in the buffer region, the turbulent kinetic energy budget is known not to be in equilibrium (i.e., $\epsilon \neq \Gamma\tau_t$) and must include its own turbulent flux-transport terms [18] that need not be identical to those in the cospectral budget. These TKE flux transport terms are dissipated in the buffer region previously discussed because production of turbulent kinetic energy generally exceeds the local dissipation rate (by as much as a factor of 2 depending on the Reynolds number), they become negligible in the intermediate region, but then they function as a source term balancing ϵ near the centerline region. Not withstanding these issues, the modeled $\sigma_w^+ = \sigma_w/u_\tau$ profiles appear to exhibit patterns that do not deviate appreciably from measurements (i.e., within 10%) except near the centerline and in the buffer region. Also, both measured and modeled σ_w^+ reveal comparably weak Re dependence (Re varied by more than three decades in the σ_w^+ comparisons in Fig. 6).

III. DISCUSSION AND CONCLUSION

Previous analytical models for pressure-driven pipe flows at high Re included, at minimum, three empirical (but Re-independent) constants that were *a priori* fitted to data [55]. The proposed cospectral budget has also well-defined constants—the Rotta similarity constant $C_R = 1.8$ and the exponential spectral correction parameter β_d, which varies

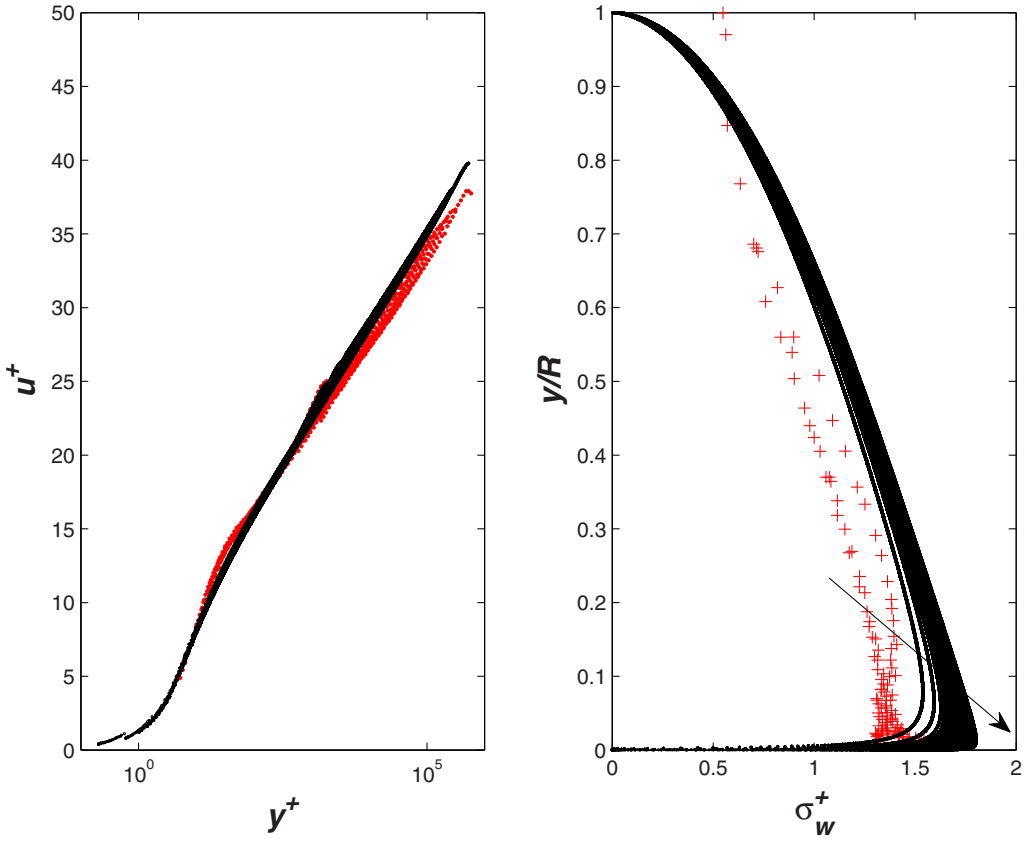

FIG. 6. (Color online) Left panel: Same as Fig. 4 but for all profiles reported in the Superpipe experiment [5,6]. Right panel: measure $\sigma_w^+ = \sigma_w/u_\tau$ (plus symbol) for the highest and lowest Re and modeled σ_w^+ for all the reported profiles [5,6] are also shown. The arrow direction indicates increasing Re.

with Re_λ, are both constrained and can be inferred independent of the cospectral model. In fact, it was shown here that C_R can be derived from the von Kármán and Kolmogorov constants. However, at the low-wave-number end, a third constant γ_p that describes the decay of energy for $kR \to 1$ remains empirically specified, although its value appears to be close to the one predicted from the von Kármán spectrum at low wave numbers.

As already discussed, another class of analytical models links the mean velocity profile to the spectrum of turbulence [11] using two strong assumptions: (i) momentum transporting eddies cannot be larger than y, and (ii) the kinetic energy spectrum of turbulence is responsible for turbulent shear stress production. The cospectral approach proposed here relaxes the first assumption and entirely departs from the second. In the proposed model, all wave numbers contribute to $F_{wu}(k)$ at any given y/R. Furthermore, the cospectral budget reveals that the vertical velocity spectrum, not the turbulent kinetic energy spectrum, is responsible for the production of $\overline{u'w'}$. This point is significant given that the turbulent kinetic energy spectrum is known to exhibit different scaling laws at low wave numbers when compared to its $E_{ww}(k)$ counterpart. Some of these differences are also attributed to inactive eddy contributions to the longitudinal velocity spectrum $E_{uu}(k)$ that are absent in $E_{ww}(k)$. For example, studies on individual velocity component spectra in the vicinity of $ky = 1$ suggest that $E_{uu}(k)$ (the main contributor to the turbulent kinetic energy) approximately scales as k^{-1} while $E_{ww}(k)$ approximately scales as k^0, as discussed elsewhere [56,57].

ACKNOWLEDGMENTS

G.K. acknowledges support from the National Science Foundation (NSF-AGS-1102227), the United States Department of Agriculture (2011-67003-30222), the US Department of Energy (DOE) through the office of Biological and Environmental Research (BER)Terrestrial Ecosystem Science (TES) Program (DE-SC0006967), and the Binational Agricultural Research and Development (BARD) Fund (IS-4374-11C).

[1] A. Perry and C. Abell, J. Fluid Mech. **79**, 785 (1977).
[2] A. Perry and M. Chong, J. Fluid Mech. **119**, 106 (1982).
[3] A. Perry and J. Li, J. Fluid Mech. **218**, 405 (1990).
[4] C. Swanson, B. Julian, G. Ihas, and R. Donnelly, J. Fluid Mech. **461**, 51 (2002).
[5] B. McKeon, M. Zagarola, and A. Smits, J. Fluid Mech. **538**, 429 (2005).

[6] B. McKeon, C. Swanson, M. Zagarola, R. Donnelly, and A. Smits, J. Fluid Mech. **511**, 41 (2004).
[7] B. McKeon and J. Morrison, Philos. Trans. R. Soc. A. **365**, 771 (2007).
[8] J. Allen, M. Shockling, G. Kunkel, and A. Smits, Philos. Trans. R. Soc. A **365**, 699 (2007).
[9] G. Barenblatt and A. Chorin, SIAM Rev. **40**, 265 (1998).
[10] N. Goldenfeld, Phys. Rev. Lett. **96**, 044503 (2006).
[11] G. Gioia, N. Guttenberg, N. Goldenfeld, and P. Chakraborty, Phys. Rev. Lett. **105**, 184501 (2010).
[12] V. Yakhot, S. Bailey, and A. Smits, J. Fluid Mech. **652**, 65 (2010).
[13] A. N. Kolmogorov, Proc. R. Soc. London A **434**, 9 (1991).
[14] U. Frisch, *Turbulence* (Cambridge University Press, Cambridge, UK, 1995), p. 296.
[15] G. Katul, A. Porporato, C. Manes, and C. Meneveau, Phys. Fluids **25**, 091702 (2013).
[16] P. Davidson, *Turbulence: An Introduction for Scientists and Engineers* (Oxford University Press, New York, 2004), p. 651.
[17] J. G. M. Eggels, F. Unger, M. Weiss, J. Westerweel, R. Adrian, R. Friedrich, and F. Nieuwstadt, J. Fluid Mech. **268**, 175 (1994).
[18] S. Pope, *Turbulent Flows* (Cambridge University Press, Cambridge, UK, 2000), p. 771.
[19] W. Bos, H. Touil, L. Shao, and J. Bertogli, Phys. Fluids **16**, 3818 (2004).
[20] G. G. Katul, D. Li, M. Chamecki, and E. Bou-Zeid, Phys. Rev. E **87**, 023004 (2013).
[21] B. Launder, G. Reece, and W. Rodi, J. Fluid Mech. **68**, 537 (1975).
[22] J. Rotta, Progr. Aerospace Sci. **2**, 1 (1962).
[23] K. Choi and J. Lumley, J. Fluid Mech. **436**, 59 (2001).
[24] U. Schumann and G. Patterson, J. Fluid Mech. **88**, 711 (1978).
[25] P. Durbin, J. Fluid Mech. **249**, 465 (1993).
[26] L. Onsager, Il Nuovo Cimento **6**, 279 (1949).
[27] S. Corrsin, Phys. Fluids **7**, 1156 (1964).
[28] G. Batchelor, J. Fluid Mech. **5**, 113 (1959).
[29] S. Corrsin, J. Fluid Mech. **11**, 407 (1961).
[30] R. H. Kraichnan, Phys. Fluids **11**, 945 (1963).
[31] Y.-H. Pao, Phys. Fluids **8**, 1063 (1965).
[32] R. Hill, J. Fluid Mech. **88**, 541 (1978).
[33] L. Danaila and R. Antonia, Phys. Fluids **21**, 111702 (2009).
[34] D. Cava and G. Katul, Bound. Layer Meteorol. **145**, 351 (2012).
[35] H. Tennekes and J. Lumley, *A First Course in Turbulence* (MIT Press, Cambridge, MA, 1972), p. 300.
[36] B. Kader and A. Yaglom, J. Fluid Mech. **212**, 637 (1990).
[37] M. Raupach, J. Fluid Mech. **108**, 363 (1981).
[38] J. Lumley, Phys. Fluids **10**, 855 (1967).
[39] S. Saddoughi and S. Veeravalli, J. Fluid Mech. **268**, 333 (1994).
[40] T. Ishihara, K. Yoshida, and Y. Kaneda, Phys. Rev. Lett. **88**, 154501 (2002).
[41] A. Townsend, *The Structure of Turbulent Shear Flow* (Cambridge University Press, Cambridge, 1976), p. 429.
[42] I. Marusic, J. P. Monty, M. Hultmark, and A. J. Smits, J. Fluid Mech. **716**, 716 (2013).
[43] D. O. Martinez, S. Chen, G. D. Doolen, R. H. Kraichnan, L. Wang, and Y. Zhou, J. Plasma Phys. **57**, 195 (1997).
[44] J. Meyers and C. Meneveau, Phys. Fluids **20**, 065109 (2008).
[45] Z. Rongrong and A. Smits, J. Fluid Mech. **576**, 457 (2007).
[46] A. N. Kolmogorov, J. Fluid Mech. **13**, 82 (1962).
[47] F. Anselmet, Y. Gagne, E. Hopfinger, and R. Antonia, J. Fluid Mech. **140**, 63 (1984).
[48] K. Sreenivasan and R. Antonia, Annu. Rev. Fluid Mech. **29**, 435 (1997).
[49] J. Qian, Phys. Fluids **27**, 2229 (1984).
[50] G. Falkovich, Phys. Fluids **6**, 1411 (1994).
[51] D. Donzis and K. Sreenivasan, J. Fluid Mech. **657**, 171 (2010).
[52] A. Bershadskii, Phys. Fluids **20**, 085103 (2008).
[53] M. Hallbck, J. Groth, and A. Johansson, in *Advances in Turbulence 3*, edited by A. Johansson and P. Alfredsson (Springer, Berlin, 1991), pp. 414–421.
[54] A. V. Johansson and M. Hallbck, J. Fluid Mech. **269**, 143 (1994).
[55] V. S. L'Vov, I. Procaccia, and O. Rudenko, Phys. Rev. Lett. **100**, 054504 (2008).
[56] G. Katul, A. Porporato, and V. Nikora, Phys. Rev. E **86**, 066311 (2012).
[57] T. Banarjee and G. Katul, Phys. Fluids **25**, 125106 (2013).